Bulletin of the Seismological Society of America, Vol. 103, No. 6, pp. 3347–3353, December 2013, doi: 10.1785/0120130073

Short Note

High-Frequency Directivity Effect for an M_w 4.1 Earthquake, Widely Felt by the Population in Southeastern France

by Françoise Courboulex, Alain Dujardin, Martin Vallée,* Bertrand Delouis, Christophe Sira, Anne Deschamps, Laetitia Honoré, and François Thouvenot

Abstract We document a moderate earthquake in the French Alps (26 February 2012 M_w 4.1) that has been much more distinctly felt south of the event than north of it. This discrepancy was especially clear in the two large cities of Nice and Grenoble, both situated at 100 km from the epicenter. This observation was confirmed by ground-motion measurements that were eight times larger in one city than in the other one, for the same site conditions. Using a time-domain deconvolution between the broadband recordings of the mainshock and an aftershock used as empirical Green's functions, we show that the rupture process of this event had a strong directivity effect toward a direction of N155° ± 5 on an ~2 km long fault, detectable only at frequencies higher than 1 Hz. The fault size and direction are in good accordance with the location of the aftershocks. Despite the various possible contributions leading to high-frequency amplification, we show here that this simple directivity effect controlled the intensity felt by the population and the acceleration measured in the cities.

Introduction

Directivity of the rupture process is a parameter of the seismic source that plays an important role in the generation of ground motions and thus in structural damage. In the direction of directivity, that is, at stations that see the rupture coming, the duration of the apparent source-time function (ASTF) is shorter than the real duration of the process on the fault. This is the opposite at antidirective stations, in which the ASTF is longer than the real source duration. As a consequence, at equal epicentral distances and for the same site conditions, the ground motions will be higher in the direction of directivity.

The directivity effect has been extensively studied by many authors (see Ben-Menahem [1961] and Boatwright and Boore [1982], among many other papers on directivity) and more recently has also been introduced into high-frequency simulations (Ruiz *et al.*, 2011). Some attempts to include the variability due to directivity in ground-motion prediction equations (GMPEs) as well as in probabilistic seismic-hazard assessment have been proposed by different authors (Somerville *et al.*, 1997; Spagnuolo *et al.*, 2012).

Directivity has been particularly well studied on recent huge earthquakes like the 2004 Sumatra event or the 2011 Tohoku event (Vallée, 2007; Ammon *et al.*, 2011; Ide *et al.*, 2011), but also on moderate-sized earthquakes like the 2009 M_w 6.3 L'Aquila earthquake (Chiarabba *et al.*, 2009) or the M_w 6.1 and M_w 7 2010–2011 Christchurch sequences (Holden, 2011).

Whereas small events are often considered as point sources, it has been proven that the directivity effect still exists for earthquakes with magnitude ≤ 5 (Courboulex *et al.*, 1999; Hough, 2001; McGuire, 2004; Boatwright, 2007; Kane *et al.*, 2013). The directivity effect studied in this paper could be only seen as one more example of the persistence of directivity effects for small earthquakes. However, this case is more interesting as (1) it reveals that these effects can still be very important at distances of the order of 100 km, which was not clear before (Singh *et al.*, 2011) and (2) these effects have been consistently recorded by the population and by the seismic instruments.

During the night of 26 February 2012, the inhabitants of the Ubaye Valley in the French Alps were woken by the brutal vibration due to the Barcelonnette earthquake. This earthquake occurred in one of the most seismically active regions in the French Alps, which has been hit in 2003–2004 by an earthquake swarm with no less than 16,000 events (Jenatton *et al.*, 2007). The February 2012 earthquake occurred about 10 km to the northwest of this swarm. It was followed by around 1000 smaller events, currently under study (see Data and Resources for a link to the Sismalp web page). We do not aim here at providing a comprehensive view of the whole

*Now at Institut de Physique du Globe de Paris, Sorbonne Paris Cité, Univ Paris Diderot, 7 UMR 7154 CNRS, 75005 Paris, France.

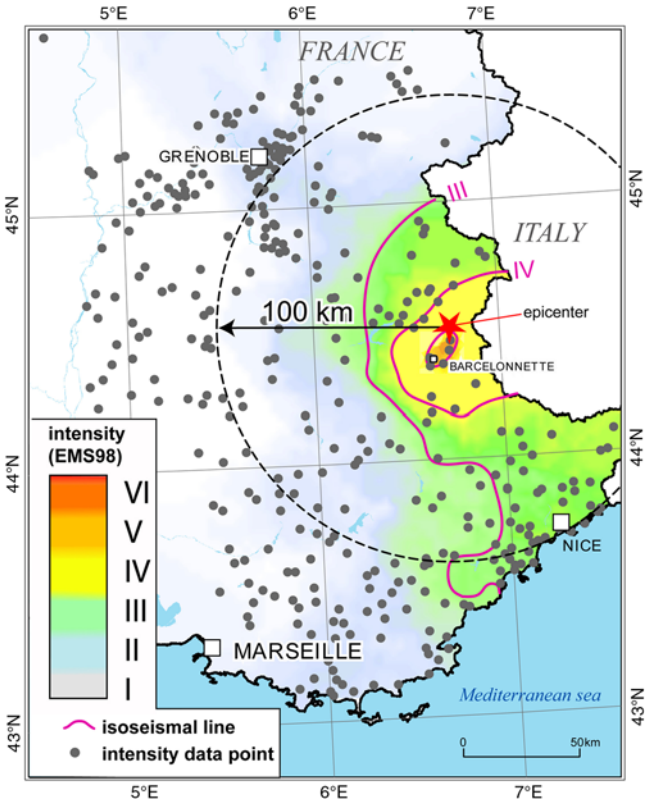

Figure 1. Macroseismic intensities collected for the M_w 4.1 26 February 2012 earthquake (source BCSF). The star indicates the earthquake epicenter and the dots show where the information has been collected. The interpolation and the determination of isoseismal lines have been made automatically by kriging. The earthquake was much more distinctly felt toward the south than toward the north. This is especially clear in the cities of Nice and Grenoble, both situated 100 km from the epicenter. The color version of this figure is available only in the electronic edition.

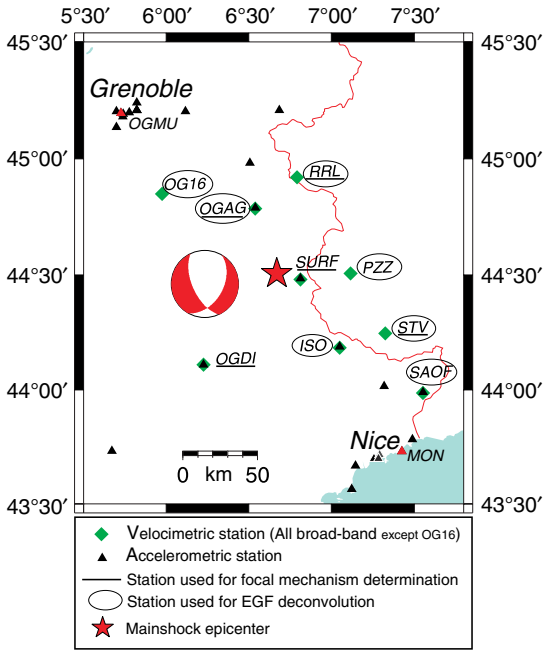

Figure 2. Map of the seismological stations used in this study. Accelerometric stations are represented by triangles and velocimeter stations by squares. The stations that are used for determination of the focal mechanism using waveform fitting are underlined and the ones that are used for directivity analysis using empirical Green's functions are surrounded. The star indicates the epicenter. The color version of this figure is available only in the electronic edition.

earthquake sequence but specifically concentrate on the mainshock and its relations with the early aftershocks. We have used three types of data, providing complementary information: macroseismic intensities (Fig. 1) collected by the French central seismological office (BCSF), accelerometric data from the permanent accelerometric network, and seismograms from the Italian and French broadband and short-period networks (Fig. 2).

Evidences from Macroseismic Intensities

The 2012 Barcelonnette event was strongly felt by the population situated in the villages around the epicenter, and caused some light damage to houses (25 chimneys were partially damaged, and a great deal of nonstructural damage was detected). The macroseimic values of intensity were estimated using the European Macroseismic Scale 1998 (EMS98) by the BCSF. Information has been obtained for 493 cities (small dots on Fig. 1) from 2314 testimonies (270 collective and 2044 individual forms). A maximum intensity of V–VI was reached in the southern part of the epicentral region (Fig. 1). This event occurred in a mountainous area populated only by villages or small cities, the two largest cities (Grenoble and Nice) being both situated about 100 km from the epicenter. In these cities, the number of data collected was very different: 279 individual testimonies were collected in Nice and only four in Grenoble, which is a first result in itself. A rapid inspection of the intensity values estimated in both cities (Fig. 1) immediately proved the fact that this event was much more felt in Nice and its surroundings than in Grenoble. This discrepancy between macroseismic intensities toward the northwest and toward the southeast was confirmed at any epicentral distance. In order to understand these differences, we first checked whether the recorded ground motion was in accordance with what the population had felt.

Seismic Data and Ground-Motions Measurements

The area under study is very close to the French–Italian border and a detailed analysis requires the combination of seismological networks from both countries. We make use here of the French broadband (RLBP) and accelerometric (RAP) networks, as well as of the regional seismic network of northwestern Italy (RSNI). One station from the Sismalp local network (OG16) has also been included. All the stations used in the study are shown in Figure 2. The cities of Nice and Grenoble are particularly well instrumented because site effects are studied in both cities using permanent urban stations.

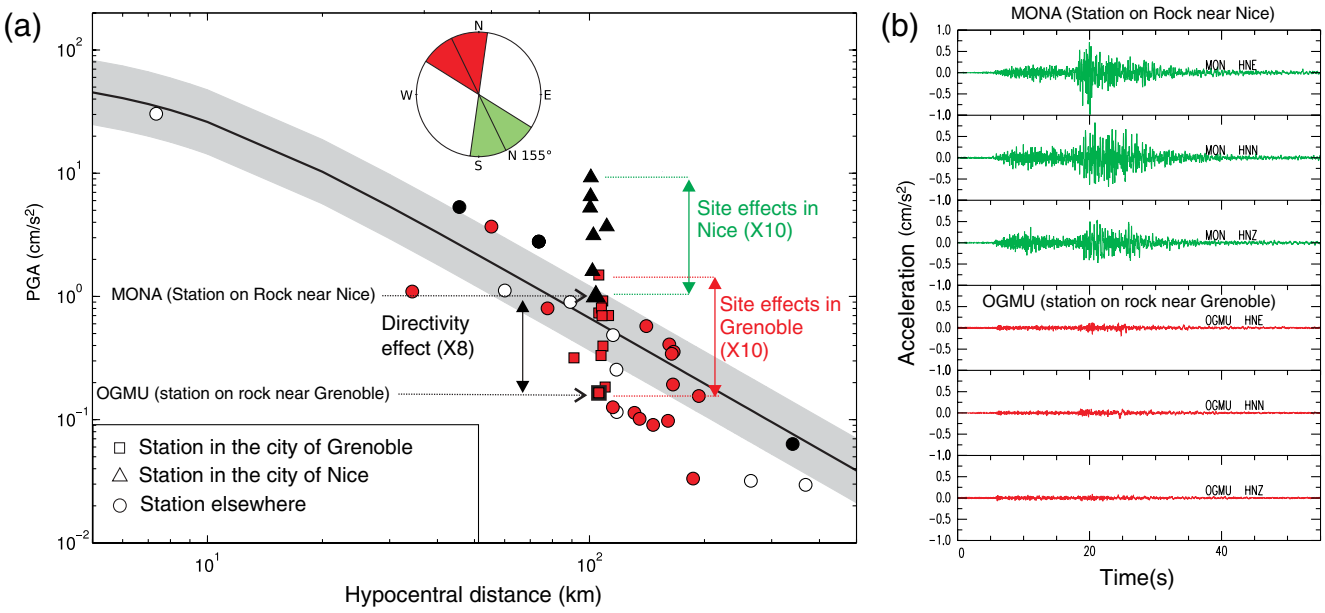

Figure 3. (a) Peak ground acceleration (PGA) values (maximum between horizontal and vertical components) are plotted against hypocentral distance. Squares indicate values in the city of Grenoble, triangles in the city of Nice, and circles for other locations. In order to evidence the azimuthal differences, the symbols that represent the values at stations that are in an azimuth N155° ± 33° are filled in light and the ones in the opposite direction are filled in dark. The other ones are white. The ground-motion prediction equation (GMPE) of Akkar and Bommer (2010) for rock sites conditions is represented by a black line for the median value and gray area that represents the 16th and 84th percentiles ($\pm\sigma$, one standard deviation for a logarithmic representation). (b) Accelerograms recorded at two good rock-site stations OGMU in Grenoble and MON in Monaco (see station location on Fig. 2) are represented at the same scale. The color version of this figure is available only in the electronic edition.

We simply plotted on Figure 3a the peak ground acceleration (PGA) values recorded at each accelerometric station as a function of the epicentral distance. The largest value between both horizontal components was chosen. In order to highlight the differences obtained in both cities, the PGA values obtained at stations situated in the city of Grenoble are represented by squares, the one obtained at stations in Nice by triangles, and the other ones by circles (Fig. 3a). Note that we only selected stations situated on the ground and excluded stations in buildings.

In each city, the intraevent variability of the PGA value (variability from one station to another one) reaches an approximate value of 10. This factor has been evidenced in Grenoble and in Nice and is explained by many authors as due to site effects (i.e., Semblat *et al.*, 2000; Lebrun *et al.*, 2001). If now we consider the PGA values obtained on the two stations in both cities that are considered as good rock-site stations (OGMU in Grenoble and MON in Monaco that is close to Nice, see Fig. 2), we obtain a value eight times larger in Nice than in Grenoble (Fig. 3a,b). Without further information, we cannot state whether this discrepancy is due to a difference in the crustal wave propagation, or to a directional source effect.

Then, taking the values recorded in both cities together, we obtain an intraevent variability of the PGA at 100 km that reaches a factor of 80 between the largest and the smallest value. In order to have a base of comparison, we plotted on the same figure GMPEs proposed by Akkar and Bommer (2010) for rock conditions, which appear to be generally well adapted to the French territory (Beauval *et al.*, 2012). The median value predicted by the GMPE is in good accordance with the overall median value of real data, but the variability obtained is much larger for this event than what was predicted by the ±1 sigma interval (Fig. 3a).

On Figure 3a, we have also tried to evidence the general azimuthal dependency of the PGA at a given distance. We observe that most of the PGA values that are higher than the GMPEs come from stations situated toward the southeast (the exact value that is chosen for the azimuth dependency will be explained further on in this paper). In the opposite direction most of the stations exhibit PGA values lower than the GMPEs. This result is interesting but cannot be taken as a proof as site effects have not been removed.

We now investigate in detail the source process of this event, first using waveform modeling to determine the focal mechanism and M_w value and then using an empirical Green's function approach.

Source Characteristics Using Broadband Seismograms

The focal mechanism was determined using a grid search on the strike, dip, and rake parameters assuming a double-couple point source and five near-source stations (Fig. 2). The broadband records were integrated to displacement and band-pass filtered between 0.03 and 0.8 Hz.

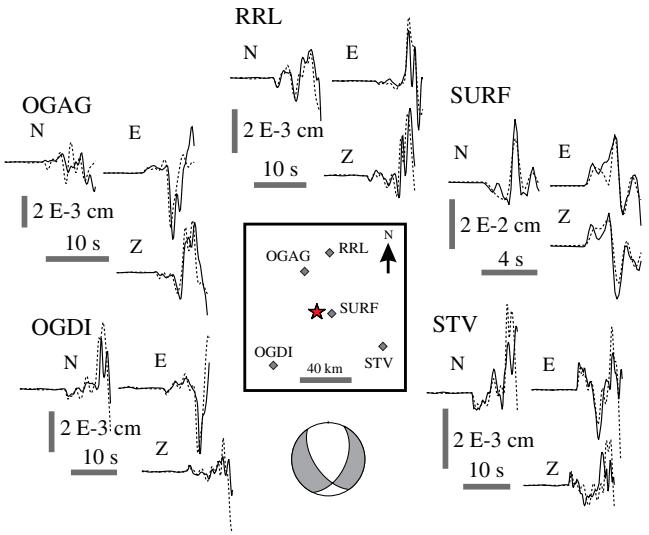

Figure 4. Focal mechanism of the mainshock (strike = 155°, dip = 60°, rake = −125°, depth = 7 km] and moment (M_w 4.15) obtained by waveform inversion of near-source stations. The observed and computed seismograms are drawn in displacement, in continuous gray and dashed black lines, respectively. All signals are band-pass filtered between 0.03 and 0.8 Hz. The star indicates the epicenter determined by Sismalp network (latitude = 44.496°, longitude = 6.664°). The color version of this figure is available only in the electronic edition.

Synthetic seismograms were computed using the wavenumber integration approach of Bouchon (1981) with a 1D layered velocity model used routinely by the Observatory of Grenoble for earthquake locations (Table 1, V_P/V_S = 1.73). The high-cut frequency, 0.8 Hz, is taken rather high to obtain more accuracy on the focal parameters. However, due to the difficulty modeling late arrivals on the seismograms with a simple 1D velocity model, records are cut a short time after the *S*-wave arrival (Fig. 4). Focal depth was also explored with a grid search. The final parameters are [strike, dip, rake] = [155°, 60°, −125°], depth = 7 km, and M_w 4.15.

The focal mechanism obtained is in good agreement with the extensional strike-slip regime in the northwest Mercantour margin and inner part, as evidenced by Jenatton *et al.* (2007) and Larroque *et al.* (2009), characterized by a northeast–southwest to east–west direction of extension.

In the frequency range used, 0.03–0.8 Hz, which is dominated by periods of the order of a few seconds (Fig. 4), no particular directivity can be observed and the point source model is adequate. In the next section, we will try to work at higher frequencies in order to evidence a possible directional effect of the source.

High-Frequency Analysis Using Empirical Green's Functions

An efficient way to analyze the directivity effect of a small earthquake is to use an empirical Green's function (EGF) deconvolution approach. Indeed, a numerical Green's function computed with a standard velocity model is not accurate enough to represent the path effect at sufficiently high frequencies. The empirical Green's function approach was primarily proposed by Hartzell (1978), who used the signal of a smaller event to represent the Green's function of the main earthquake. The usual requisites for the smaller event are to be one or, better, two degrees of magnitude smaller than the mainshock and to have a similar location and focal mechanism.

Table 1
Velocity Model

Velocity (*P* wave) km/s	Depth (Relative to Sea Level) km
5.30	0
5.92	3
6.60	27
8.00	35

We have selected four earthquakes that best fit these criteria and tested them in the deconvolution process. The first one had certainly a complex source-time function that prevented us from obtaining a good fit. The two other ones did not have a sufficient good signal-to-noise ratio (SNR) at each station. We finally selected the 27 February aftershock that occurred at 23:05 as suitable for EGFs because it gathered all the necessary conditions (same location, depth, good SNR, and a magnitude significantly lower than the mainshock) and was determined, with the same method as for the mainshock, to have a similar focal mechanism and a value of M_w equal to 2.3.

We used the deconvolution method developed by Vallée (2004) that stabilizes the classical deconvolution between the mainshock and the EGF in order to obtain more reliable ASTFs. The following physical constraints are introduced: the ASTF obtained must be causal and positive, and its integral, which corresponds to the moment ratio between the mainshock and the aftershock, must be the same for all stations. This last constraint on the moment stabilizes the process.

Deconvolving such a small event is not an easy task because we aimed to reproduce high frequencies and thus the small differences in the location, depth, and the focal mechanism between the mainshock and the small event used as an EGF can be problematic. *P* and *S* waves have also to be well separated. We therefore did not directly use the closest broadband station called SURF, which was used in the last paragraph for low-frequency broadband analysis. We also rejected the stations too far away in order to keep an excellent SNR for the EGF recordings. We finally kept seven stations (Fig. 2) for which we obtained an ASTF solution that produces a fit to the real signal of 90%: six broadband stations (three in France and three in Italy) and one short-period station (equipped with a L4C-1 Hz sensor) from the local Sismalp network. The use of short-period stations was possible because we worked only on frequencies between 0.5

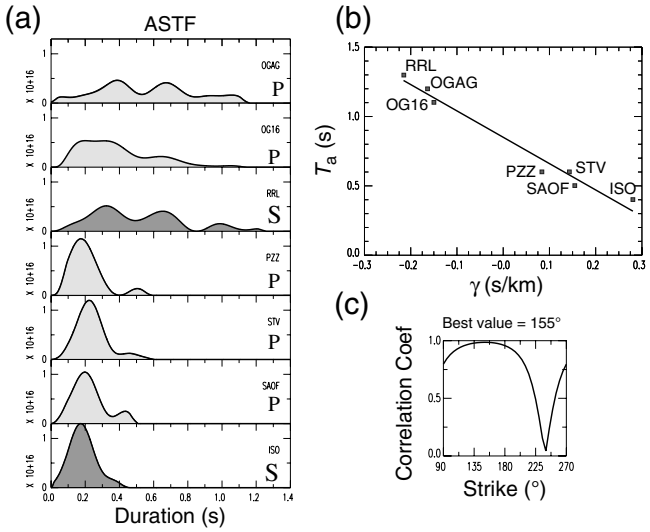

Figure 5. (a) Apparent source-time functions (ASTFs) in light gray for *P* waves, and in dark gray for *S* waves. (b) Best linear fit (see correlation coefficient on *c*) obtained between the ASTF durations and $\gamma = \sin(\psi)\cos(\theta - \theta_0)/c$, which indicates that the rupture propagated toward the direction N155° during about 0.85 s.

and 10 Hz and also because we used a method of deconvolution, which inherently removes the instrumental response.

The way to choose the best ASTF for each station is explained in Vallée (2007). In order to avoid overinterpretation of nonsignificant details of the ASTFs, we worked both on vertical and transverse components. Vertical components were easier to use because the isolation of a simple *P* wave was generally unambiguous on both the mainshock and aftershock recordings. Nevertheless, the *P* waves at two stations were not clear enough to be used, maybe because of the focal mechanism effect. At these two stations, we succeeded in using transverse components because the *S* waves were particularly clearly separated from the other wave trains.

The ASTFs obtained for the seven stations clearly show that the rupture process was not simple (Fig. 5a). While the stations situated toward the north exhibit ASTFs with durations between 1.2 and 1.4 s, the ASTFs obtained for the stations in the south are much shorter (~0.4 s). As expected, the complexity of the source, which probably includes two or three subevents, is much better seen on stations to the north. The amplitude of the ASTFs obtained in the south is about three times larger than the ones obtained in the north (Fig. 5a). This is in good accordance with the ratio we obtain between the peak values of the signals in displacement (peak ground displacement obtained by double integration of the accelerograms) in both cities for stations on rock site conditions. This means that all the variability of the amplitude can be explained by a directivity effect of the rupture toward a general southern direction.

The ASTF obtained from *P* and *S* waves are represented on Figure 5a. In order to refine the horizontal direction of directivity and to propose a model that fits the data, we assume a simple line source with unilateral rupture propagation. Defining T_a as the ASTF duration at each station, we have the relation

$$T_a = T_r - \sin\Psi L \frac{\cos(\theta - \theta_0)}{c}, \qquad (1)$$

in which θ and θ_0 are the azimuth of the station and the rupture propagation, respectively, Ψ is the takeoff angle of the ray, T_r is the real duration of the rupture process, L is the length of the fault, and c is the wave velocity around the source (we considered here that $V_P = 5.9$ km/s and $V_P/V_S = 1.73$). We searched for the best value of L and T_r to fit the linear equation (1) by a systematic variation of θ_0 by steps of 5°. Figure 5b and 5c show that the best fit (correlation of 98%) is obtained for a rupture that propagates toward the direction N155° during 0.85 ± 0.03 s on a 2 ± 0.15 km long fault. The angle of the directivity and the duration of the rupture process we found are very stable. The length of the fault is less constrained and more dependent on the wave velocities that are chosen in the source region. The resulting rupture velocity is rather low, around 2.3 km/s, and the static stress drop computed from seismic moment and rupture length is ~0.6 MPa.

Relation with Aftershocks Location

We used 23 stations at less than 150 km from the epicentral area (three of them are at less than 12 km), which warrants the observation of crustal phases: 20 French stations (short period and broadband Sismalp and RESIF networks) and three Italian stations. Two more short-period stations were installed a few days after the mainshock close to the epicenters (less than 6 km).

For this study, seismograms were first picked manually and then we used hypref2005, a modified version of the hypo71 program (Lee and Lahr, 1975) which takes second arrivals and station altitudes into account. We adopted the velocity model of Table 1 which has been used routinely at Observatoire de Grenoble over the last 30 years for locating earthquakes in the Alps. We eventually formed travel-time differences from *P* and *S* picks, and used the HYPODD program (Waldhauser and Ellsworth, 2000) to improve location precision. In the HYPODD procedure, we selected event pairs with at least eight phase links, which excludes many events recorded by too few stations. Figure 6 shows the epicenters of the mainshock and 39 aftershocks, which occurred in the following five days and were located with HYPODD. The aftershock, which recordings were used in the last paragraph as empirical Green's functions, is represented by a bold circle. Events occurred in the crystalline basement, in the 2–9 km depth range (referred to sea level). The early aftershock zone (Fig. 6) forms an ~2 km long alignment that trends ~N150°–160°, which is in good accordance with the fault length we have previously obtained from the directivity analysis. All the aftershocks of the sequence occurred south

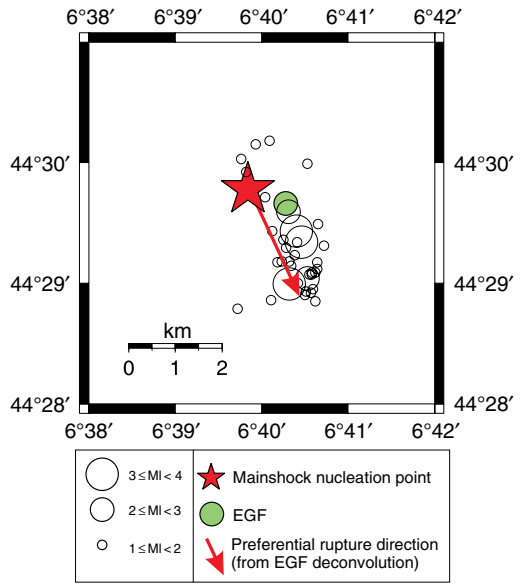

Figure 6. Mainshock nucleation point (star) and 39 aftershocks locations from HYPODD procedure for the first five days ($M_l \geq 1$). The arrow indicates the directivity of the rupture process and the length of the fault that were obtained from the EGF deconvolution analysis. The color version of this figure is available only in the electronic edition.

to the epicenter, which may suggest that the fault could not be activated to the north.

Conclusions

We have shown that the 26 February 2012 Barcelonnette M_w 4.1 earthquake occurred on an ~2 km normal fault dipping west and that the rupture process had a dominant directivity effect toward the direction N155°. This result is in good accordance with the aftershocks distribution. The directivity effect of this event is responsible for an important asymmetry of the macroseismic intensity map at close and far distances and for a large increase of the PGA values for directive stations (at least eight times larger, for the same site conditions).

This study underlines the fact that directivity has to be taken into account for the analysis of historical earthquakes, because it may lead to an over- or underestimation of the magnitude. It has also to be carefully taken into account in ground-motion predictions because it significantly increases the variability of the expected PGA values.

Data and Resources

Strong-motion and broadband seismic data from the French broadband network (RESIF), the French accelerometric network (RAP), and broadband network (RLBP) were obtained through the RESIF data distribution facility publicly available online (http://www.resif.fr; last accessed June 2013). Italian Broadband data can be retrieved through the Eida portal (http://eida.rm.ingv.it; last accessed June 2013). Macroseismic data can be retrieved through the French central seismological office (BCSF) website (http://www.franceseisme.fr/; last accessed June 2013). The study of the aftershocks of the Barcelonnette event can be followed on http://sismalp.obs.ujf-grenoble.fr/cases/stpaul/stpaul.html (last accessed June 2013).

Acknowledgments

We thank Christophe Maron for his help in checking the data quality and all the persons in charge of the permanent seismological networks (French accelerometric network [RAP], French broadband network [RESIF], French short-period network [Sismalp], regional seismic network of northwestern Italy [RSNI]) for free and easy access to the data. This paper has been improved by fruitful discussion with Mathieu Causse and Paola Traversa, and greatly enhanced by the remarks of two anonymous reviewers. Alain Dujardin's Ph.D. thesis is supported by the SIGMA-EDF project.

References

Akkar, S., and J. J. Bommer (2010). Empirical equations for the prediction of PGA, PGV, and spectral accelerations in Europe, the Mediterranean region, and the Middle East, *Seismol. Res. Lett.* **81,** 783–793.

Ammon, J., T. Lay, H. Kanamori, and M. Cleveland (2011). A rupture model of the 2011 off the Pacific coast of Tohoku Earthquake, *Earth Planets Space* **63,** 693–696.

Beauval, C., H. Tasan, A. Laurendeau, E. Delavaud, F. Cotton, P. Guéguen, and N. Kuehn (2012). On the testing of ground-motion prediction equations against small-magnitude data, *Bull. Seismol. Soc. Am.* **102,** 1994–2007.

Ben-Menahem, A. (1961). Radiation of seismic surface-waves from finite moving sources, *Bull. Seismol. Soc. Am.* **51,** 401–435.

Boatwright, J. (2007). The persistence of directivity in small earthquakes, *Bull. Seismol. Soc. Am.* **97,** 1850–1861.

Boatwright, J., and D. M. Boore (1982). Analysis of the ground accelerations radiated by the 1980 Livermore Valley earthquakes for directivity and dynamic source characteristics, *Bull. Seismol. Soc. Am.* **72,** 1843–1865.

Bouchon, M. (1981). The rupture mechanism of the Coyote Lake earthquake of August 6, 1978 inferred from near field data, *Bull. Seismol. Soc. Am.* **71,** 858–871.

Chiarabba, C., A. Amato, M. Anselmi, P. Baccheschi, I. Bianchi, M. Cattaneo, G. Cecere, L. Chiaraluce, M. G. Ciaccio, P. De Gori, G. De Luca, M. Di Bona, R. Di Stefano, L. Faenza, A. Govoni, L. Improta, F. P. Lucente, A. Marchetti, L. Margheriti, F. Mele, A. Michelini, G. Monachesi, M. Moretti, M. Pastori, N. Piana Agostinetti, D. Piccinini, P. Roselli, D. Seccia, and L. Valoroso (2009). The 2009 L'Aquila (central Italy) M_w 6.3 earthquake: Main shock and aftershocks, *Geophys. Res. Lett.* **36,** no. L18308, doi: 10.1029/2009GL039627.

Courboulex, F., N. Deichmann, and J. C. Gariel (1999). Rupture complexity of a moderate intraplate earthquake in the Alps: The 1996 *M* 5 Epagny-Annecy earthquake, *Geophys. J. Int.* **139,** 152–160.

Hartzell, S. H. (1978), Earthquake aftershocks as Green's functions, *Geophys. Res. Lett.* **5,** 1–4.

Holden, C. (2011). Kinematic source model of the 22 February 2011 M_w 6.2 Christchurch earthquake using strong motion data, *Seismol. Res. Lett.* **82,** 783–788.

Hough, S. E. (2001). Empirical Green's function analysis of recent moderate events in California, *Bull. Seismol. Soc. Am.* **91,** 456–467.

Ide, S., A. Baltay, and G. C. Beroza (2011). Shallow dynamic overshoot and energetic deep rupture in the 2011 M_w 9.0 Tohoku-Oki earthquake, *Science* **332,** 1426–1429.

Jenatton, L., R. Guiguet, F. Thouvenot, and N. Daix (2007). The 16,000-event 2003–2004 earthquake swarm in Ubaye (French Alps), *J. Geophys. Res.* **112,** no. B11304.

Kane, D. L., P. Shearer, B. P. Goertz-Allmann, and F. Vernon (2013). Rupture directivity of small earthquakes at Parfield, *J. Geophys. Res.* **118,** no. B009675.

Larroque, C., B. Delouis, B. Godel, and J. M. Nocquet (2009). Active deformation at the southwestern Alps–Ligurian basin junction (France–Italy boundary): Evidence for recent change from compression to extension in the Argentera massif, *Tectonophysics* **467,** 22–34.

Lebrun, B., D. Hatzfeld, and P.-Y. Bard (2001). Site effect study in urban area: Experimental results in Grenoble (France), *Pure Appl. Geophys.* **158,** 2543–2557.

Lee, W. H. K., and J. E. Lahr (1975). Hypo71: A computer program for determining hypocenter, magnitude, and first-motion pattern of local earthquakes, *U.S. Geol. Surv. Open-File Rept. 75-331*, 110 pp.

McGuire, J. J. (2004). Estimating finite source properties of small earthquake ruptures, *Bull. Seismol. Soc. Am.* **94,** 377–393.

Ruiz, J., D. Baumont, P. Bernard, and C. Berge-Thierry (2011). Modelling directivity of strong ground motion with a fractal, k–2, kinematic source model, *Geophys. J. Int.* **186,** 226–244.

Semblat, J.-F., A.-M. Duval, and P. Dangla (2000). Numerical analysis of seismic wave amplification in Nice (France) and comparison with experiments, *Soil Dynam. Earthq. Eng.* **19,** 347–362.

Singh, S. K., A. Iglesisas, M. Ordaz, X. Péres-Campos, and L. Quintanar (2011). Estimation of ground motion in Mexico City from a repeat of the $M\sim$7.0 Acambay earthquake of 1912, *Bull. Seismol. Soc. Am.* **101,** 2015–2028.

Somerville, P., N. F. Smith, W. Graves, and N. Abrahamson (1997). Modification of empirical strong ground motion attenuation relations to include the amplitude and duration effects of rupture directivity, *Seismol. Res. Lett.* **68,** 199–222.

Spagnuolo, E., A. Herrero, and G. Cultrera (2012). The effect of directivity in a PSHA framework, *Geophys. J. Int.* **191,** 616–626.

Vallée, M. (2004). Stabilizing the empirical Green function analysis: Development of the projected Landweber method, *Bull. Seismol. Soc. Am.* **94,** 394–409.

Vallée, M. (2007). Rupture properties of the giant Sumatra earthquake imaged by empirical Green's function analysis, *Bull. Seismol. Soc. Am.* **97,** 103–114.

Waldhauser, F., and W. L. Ellsworth (2000). A double-difference earthquake location algorithm: Method and application to the Northern Hayward Fault, California, *Bull. Seismol. Soc. Am.* **90,** 353–368.

Université Nice Sophia Antipolis
CNRS, IRD
Observatoire de la Côte d'Azur
250 rue Einstein
06560 Valbonne, France
courboulex@geoazur.unice.fr
(F.C., A.D., M.V., B.D., A.D., L.H.)

UMS830-BCSF,
Université de Strasbourg
EOST, CNRS
5 rue René Descartes
67084 Strasbourg, France
(C.S.)

ISTerre,
Université Joseph-Fourier (Grenoble)
CNRS, 38041, BP 53
38041 Grenoble Cedex 9
France
(F.T.)

Manuscript received 28 March 2013;
Published Online 5 November 2013